To the Graduate Council:

I am submitting herewith a thesis written by Robert L McDaniels entitled "The Effect of the Heat-Affected Zone Created by Laser-Surface Alloying on the High-Cycle Fatigue Behavior of AISI 4340 Steel." I have examined the final paper copy of this thesis for form and content and recommend that it be accepted in partial fulfillment of the requirements for the degree of Master of Science, with a major in Materials Science and Engineering.

Dr. Peter K. Liaw, Major Professor

We have read this thesis and recommend its acceptance:

Acceptance for the Council

Vice Provost and Dean of Graduate Studies

The Effect of the Heat-Affected Zone Created by Laser-Surface Alloying on the High-Cycle Fatigue Behavior of AISI 4340 Steel

A Thesis for the
Master of Science Degree
The University of Tennessee

Robert L. M^{c}Daniels
May 2002

Thesis
2002
.M242

ACKNOWLEDGEMENTS

The author would like to extend his sincerest thanks to his two advisors, Dr. Peter Liaw and Dr. Ray Buchanan, for providing the opportunity to conduct the present research. In addition, he would like to thank Steve White, Melanie Kirkham, Mike Benson, Dr. Lijia Chen, Kevin Liaw, and the other members of our group at the Department of Materials Science and Engineering, The University of Tennessee, Knoxville, TN. Without their help and hard work, this research would never have progressed this far.

The author would like to recognize the support of Dr. Mary Helen M^{c}Cay of the Center for Laser Applications, The University of Tennessee Space Institute, Tullahoma, TN.

The author would like to thank Dr. Charlie Brooks, Doug Fielden, and Greg Jones for their support and encouragement at the Department of Materials Science and Engineering, The University of Tennessee, Knoxville, TN.

This work is also supported by the National Science Foundation, the Division of Design, Manufacture, and Industrial Innovation, under Grant No. DMI-9724476, and the Combined Research-Curriculum Development Program (CRCD), under EEC-9527527, and the Integrative Graduate Education and Research Training (IGERT) Program under DGE-9987548, to the University of Tennessee, Knoxville, with Dr. D. Durham, Ms. M. Poats, Dr. W. Jennings, and Dr. L. Goldberg, as contract monitors, respectively.

ABSTRACT

The high-cycle fatigue behavior of a CrB_2-coated AISI 4340 steel subjected to four-point-bend fatigue experiments is discussed. Samples of AISI 4340 steel from several different lots were coated with CrB_2 by a laser-surface-alloying (LSA) process. The samples were then subjected to four-point-bend, high-cycle-fatigue testing. The experiments were run to failure at an R ratio of 0.1, where $R = \sigma_{min}/\sigma_{max}$, σ_{min} and σ_{max} being the minimum and maximum applied stresses, respectively. The failed samples were then subjected to Scanning Electron Microscopy (SEM) and metallography. For the Lot 1 and Lot 2 material showed slightly improved fatigue performance at some stress levels, but for the Lot 4 samples, the laser coating proved to be detrimental to the fatigue performance of the alloy. Microhardness measurements as a function of the depth from the coating surface were taken for each lot of material. The difference in fatigue performance between the various lots was explained in terms of the fracture mechanisms, microstructures, and hardness differences resulting from the LSA process.

TABLE OF CONTENTS

1.0 Project Summary 1

2.0 Introduction 2
2.1 Background 2
2.1.1 Laser-Surface Alloying (LSA) 2
2.1.2 Challenges 3
2.1.3 Critical Issues 3

3.0 Research Methods 5
3.1 Objective 5
3.2 Specimen Preparation 5
3.2.1 Substrate Selection 5
3.2.2 Laser Processing 6
3.2.3 Microhardness Sample Preparation 7
3.2.4 Fatigue Sample Preparation 7
3.2.5 Metallography Sample Preparation 8
3.3 Test Methods 8
3.3.1 Tension Testing 8
3.3.2 Microhardness Testing 8
3.3.3 Fatigue Testing 9
3.3.4 Microscopy 11

4.0 Results and Discussion 13
4.1 Microscopy 13
4.1.1 As-Received Microstructure 13
4.1.2 Laser-Coated Microstructure 13
4.2 Tensile Results 14
4.3 Microhardness 14
4.4 Fatigue Behavior 16
4.5 Fractography 17

5.0 Conclusions 19

6.0 Potential Impact of Research 20

7.0 Future Work 21

References Cited 23

Appendix 27

Vita 52

LIST OF TABLES AND FIGURES

Table 1. Composition of AISI 4340

Table 2. Properties of AISI 4340

Figure 1. Schematic of Research

Figure 2. Sketch of Specimen Geometry Detailing Dimensions and Geometric Planes of Interest

Figure 3. Test Fixture Setup with Specimen Installed

Figure 4. Bending Moment Diagram of Four-Point-Bend Test

Figure 5. Optical Micrograph of an As-Received, Untested Specimen Etched with 2% Nital

Figure 6. SEM Micrograph of an As-Received, Untested Specimen Etched with 2% Nital

Figure 7. Metallography Specimen of LC18 from Lot 1

Figure 8. Metallography Sample from Lot 2 Showing Fine Martensite Microstructure

Figure 9. A Metallography Sample from Lot 4

Figure 10. Tensile Test Results for the As-Received Samples of AISI 4340

Figure 11. Knoop Hardness Values for an As-received Sample

Figure 12. Knoop Hardness Values for a Lot 1 Sample

Figure 13. Knoop Hardness Values for a Lot 2 Sample

Figure 14. Microhardness Data for Lot 4

Figure 15. High-Cycle Fatigue Data for All Four Lots

Figure 16. High-Cycle Fatigue Data Showing Only the As-Received Lot, Lot 1 and Lot 2

Figure 17. Fractograph of LC36

Figure 18. A Higher Magnification of Figure 17

Figure 19. Fifty Micron SEM Micrograph of an As-Received Specimen

Figure 20. Twenty Micron SEM Micrograph of an As-Received Specimen

Figure 21. SEM Micrograph of a Laser-Coated Specimen from Lot 1

Figure 22. Fracture Surface of LC38, a Lot 2 Specimen

Figure 23. A Fractograph of LC38, a Lot 4 Specimen

1.0 PROJECT SUMMARY

A project to study the effects of the heat affected zone (HAZ) in AISI 4340 steel created by laser surface alloying (LSA) on high-cycle fatigue behavior has been conducted. To date, little work has been done to investigate how the heat-affected zone created by laser processing influences the fatigue behavior of high-strength, low-alloy steels, despite the tremendous influence that the heat affected zone could have on the fatigue behavior of this alloy.

This research was designed to investigate these effects and to determine which laser-processing parameters are optimal for the fatigue behavior of AISI 4340 steel. This was achieved by producing several lots of laser-processed AISI 4340 steel using different laser-processing parameters, and then subjecting the samples to high-cycle fatigue and microhardness testing. Samples of tested material from each lot were examined using scanning electron microscopy in order to establish the effects of laser processing on the microstructure of the fatigue-tested AISI 4340 steel. When these three techniques, microhardness testing, high-cycle fatigue testing, and scanning electron microscopy (SEM), are combined, a mechanistic understanding of the effect of the HAZ on the fatigue behavior of this alloy might be gained.

2.0 INTRODUCTION

2.1 BACKGROUND

2.1.1 LASER-SURFACE ALLOYING (LSA)

There has been a recognized need for many years to create materials that have surface properties that differ from those of the base material, or to modify the surface of existing materials to enhance certain properties at the surface while not affecting those properties in the subsurface region of the materials. Ceramic materials in general, and metallic borides in particular, are widely known to enhance the corrosion and wear characteristics of steels.[1] Chromium diboride has several features that make it very promising as a coating material, as it is the most resistant of the borides to corrosive-wear processes, and is resistant to chemical attack by dilute acids, bases, and molten metals.[2]

Many processes have been developed to deposit coatings onto substrates. However, the coatings are frequently prone to flaking and cracking, due to a lack of interfacial integrity with the substrate.[3] Laser-surface-alloying (LSA) has provided one solution to these problems. In the LSA process, the high energy of a laser is utilized to melt a small depth of the substrate, and the coating is then added to and alloyed with the molten metal.[3] During this process, the substrate below the heat-affected zone (HAZ) remains at a much lower temperature and acts as a heat sink. This results in cooling rates as high as 10^3–10^8 K/s and large thermal gradients, yielding rapid resolidification.[4] In the melted region, the concentration of the coating material or alloying agent is very high at the surface of the substrate, and decreases as the depth from the coating surface increases.[5] This process creates a coating layer and interface that are metallurgically bonded to the substrate and much less prone to debonding, spalling, or flaking. In the proposed research, LSA is achieved by the use of the pulsed-laser-deposition (PLD) technology, as described later.

2.1.2 CHALLENGES

It has been noted by several researchers that the weak link in the LSA coating/substrate system is the HAZ. In the HAZ, the substrate material is heated to a temperature below the melting temperature and cooled at a lower rate than the coating surface. This can lead to microstructural changes in the HAZ that are difficult to control and could have a detrimental effect on the mechanical properties of the part. Oñoro and Ranninger[6] have reported that cracks in laser welded, high-strength, low-alloy steels formed near the borderline of the fusion line and the HAZ. Lee, Kim, and Kim[7] found that the fatigue resistance was lowest in the HAZ near the fusion line. If the cooling rate of the HAZ is too slow, low-alloys steels like AISI 4340 are vulnerable to tempered martensite embrittlement, which could lead to a loss of fracture toughness and fatigue resistance.[8]

Not all materials behave the same however. Hwang et al.[9,10] found that the HAZ exhibited greater fatigue crack growth resistance than the substrate material in a cold-rolled steel, and attributed it to refinement in the microstructure of the welded zone. Tsay, Chung, and Chen[11] found similar results for D6AC steel, a high-strength, medium-carbon, low-alloy steel, and attributed it to the presence of lower bainite and tempered martensite in the microstructure of the weld region and the HAZ.

2.1.3 CRITICAL ISSUES

As can be seen from the above discussion, very little work has been done on the effect of the HAZ on the fatigue behavior of laser-processed AISI 4340. Most of the research that has been done on the HAZ has been conducted by researchers investigating the effects of welding on the HAZ, and many researchers working on laser-processed materials have ignored the HAZ. In the present research, the critical issue was to

evaluate the effects that the HAZ created by laser processing of the AISI 4340 has on the fatigue properties of the substrate.

3.0 Research Methods

3.1 Objective

The objective of the proposed research was to study the effect of the HAZ on the fatigue behavior of the AISI 4340 substrate material after it has been laser processed by LSA. This was to be accomplished by subjecting samples of AISI 4340 steel to the LSA process, then removing the coating layer by grinding and testing the remaining material in a four-point-bend fatigue experiment. The microstructure and fracture surfaces of the tested samples were then examined by scanning electron microscopy (SEM). Microstructural changes were also investigated by performing microhardness tests on the samples. A schematic of the research plan that was undertaken in study of the fatigue performance of the laser processed AISI 4340 steel is shown in Figure 1.*

3.2 Specimen Preparation

3.2.1 Substrate Selection

AISI 4340 steel was selected as the substrate material for this research. AISI 4340 is a medium-carbon, heat-treatable, oil-hardening, low-alloy steel. It has gained wide acceptance in numerous industries, such as applications including shafts, gears, aircraft landing gear, and other situations where high strength and fatigue and creep resistance are needed, even at elevated temperatures. The chemical composition of AISI 4340 is given in Table 1. The material was austenized at 843°C (1,550°F) for 20 minutes in a salt bath, oil-quenched and cooled to room temperature, and tempered at 371°C (700°F) for 2 hours. This resulted in a steel with a Knoop hardness of 500, and a microstructure of tempered martensite. The properties of AISI 4340 at this temper are given in Table 2.

*All figures and tables referenced in this manuscript appear in the Appendix, beginning on page 27.

3.2.2 LASER PROCESSING

In the Laser-Surface Alloying (LSA) process, plates of 4340 steel, 152.4 mm by 762 mm by 6.3 mm, were sandblasted, and then coated with a precursor consisting of 75 weight percent (wt%) Cr powder and 25 wt% CrB_2 powders mixed into a proprietary polymer binder that was then sprayed onto the surface of the substrate to a thickness of 100 microns.[3] Once the coating had dried, a laser beam was passed over the substrate. The laser that was chosen for this processing is a Rofin-Sinar 2 kW CW Nd:Yag laser with a fiber optic delivery and a patented[12] rectangular beam shape (750 microns by 4,000 microns).[3] The depth of the melt pool is related to the intensity of the energy that is applied to the surface.[4] The equation that describes the energy intensity is:

$$E = P/UD_b^2 \qquad (1)$$

where:

E = Energy Intensity (J/s)

P = Power output of laser (kW)

U = Translation speed of laser (mm/s)

D_b = Diameter of the beam (mm)

For the Lot 1 samples of AISI 4340, the power of the laser was maintained at 1,750 Watts, and the laser moved with a speed of 1,500 mm/min. For Lot 2, the power was maintained at 2,000 Watts, and the laser was moved at a speed of 1,500 mm/min. For Lot 4, the power was maintained at 1,400 Watts, and the laser was moved at a speed of 1,500 mm/min. Each pass of the laser is overlapped by 500 microns.[3] Once the laser processing is completed, the plates were cut into rectangular test specimens that were nominally 50 mm by 9.5 mm by 6.3 mm, with the long axis of the test specimens running perpendicular to the long axis of the original plates.

3.2.3 MICROHARDNESS SAMPLE PREPARATION

A microhardness sample was obtained from the untested portion of an as-received specimen that had not been subjected to laser processing. This sample was a cross-section of the bar, as presented in Figure 2 by plane I, and was mounted in bakelite for polishing. The sample was then polished using 320, 400, and 600 grit silicon-carbide pads and 9.5, 1.0, and 0.05 alumina slurries on a microcloth. Microhardness samples were obtained from the untested ends of selected samples from Lots 1, 2, and 4, and processed in a similar manner.

3.2.4 FATIGUE SAMPLE PREPARATION

The as-received test specimens were rectangular in shape, as shown in Figure 2. The specimens were 50 mm in length with a nominal width of 9.6 mm and thickness of 6.3 mm. The test specimens were then polished in groups of five so that their planes, as represented in Figure 2 by plane II, were parallel to one another. This was done using 320 grit and 400 grit silicon-carbide polishing pads. The two parallel planes and the plane to be placed in tension for testing, represented by plane III in Figure 2, were then polished individually using 600 grit silicon-carbide polishing pads and a microcloth with a 9.5 micron alumina slurry until a mirror finish was achieved. This process was done to minimize cracks and other machining-induced defects that could adversely affect the specimen life during fatigue testing.

In order to study the HAZ of the LSA processed specimens, the coating was removed by grinding. After that, the laser-processed HAZ test specimens were polished in a similar manner to those of the as-received lot. They were polished in groups of five using 320 grit and 400 grit silicon-carbide pads to achieve parallel planes. They were then polished individually. The sides of the specimen, plane II in Figure 2, were polished with both 600 grit silicon-carbide pads and a microcloth with a 9.5 micron alumina

slurry, while the laser-processed side, plane III in Figure 2, was simply polished with the 9.5 micron alumina slurry.

3.2.5 Metallography Sample Preparation

A metallography sample was obtained from the untested portion of an unprocessed, as-received specimen. This sample was a cross-section of the bar, as presented in Figure 2 by plane I, and was mounted in bakelite for polishing. The sample was then polished using the same procedure that is used for preparing the hardness specimen. The next step sample was to etch the specimen with 2% Nital.

In addition, once the testing has been completed on the samples that had been created for microhardness testing, the samples were etched with 2% Nital and Kallings 2 reagent in order to investigate the relationship between the microhardness indention and the microstructure of the sample.

3.3 Test Methods

3.3.1 Tension Testing

AISI is a steel that has a high hardenability, with a wide range of hardnesses and yield strengths. Two samples of as-received, unprocessed material were subjected to tension testing, so that the yield strength of this particular heat of steel could be established. The tension samples had a gage length of 31.75mm and a rectangular cross section of 6.35 mm by 3.175 mm. The tests were conducted according to ASTM E 8-00b, "Standard Test Methods for Tension Testing of Metallic Materials." [13]

3.3.2 Microhardness Testing

Samples from each lot were subjected to microhardness measurements on a Buehler MMT-3 Digital Microhardness Tester using a Knoop indenter. The samples

were prepared as metallographic specimens representing the three planes shown in Figure 2. They were mounted in bakelite, and then polished with 320, 400, and 600 grit silicon-carbide pads, and then with 9.5, 1.0, and 0.05 micron alumina slurries on a microcloth. The testing was performed in accordance with ASTM B-578-87, "Standard Test Method for Microhardness of Electroplated Coatings"[14] and ASTM E-384-99, "Standard Test Method for Microindention Hardness of Materials."[15] The microhardness testing was done with a load of 100 grams force, and a hold time of 10 s.

3.3.3 Fatigue Testing

All of the specimens were subjected to high-cycle-fatigue testing at room temperature. The test specimens were 50 mm long, 9.6 mm wide, and 6.3 mm thick, and set in the test fixture such that the outer pins were centered and 41 mm apart, and the inner pins were 20 mm apart. The experimental setup is shown in Figure 3. The tests were conducted on a Material Test System (MTS) Model 810 servohydraulic mechanical test frame, at stress levels from 300 to 1,600 MPa.

The four-point-bend tests were performed under load control, with an R ratio of 0.1, where $R = \sigma_{min}/\sigma_{max}$, and σ_{min} and σ_{max} are the minimum and maximum applied stresses, respectively. All experiments were performed at a frequency of 5 Hz and continued until the sample had failed, or the specimen life exceeded 1×10^6 cycles, at which time the experiment was suspended. The four-point-bend test was chosen because it provides a relatively broad region of the specimen that has a constant bending moment, and the stresses for a given applied load do not vary significantly between the inner pins. A graph of the bending moment diagram is given in Figure 4, which shows how the bending moment varies along the length of the sample.

For the unprocessed, as-received samples, two tests were run at each of four stress levels: 1,220, 1,350, 1,420, and 1,570 MPa, in compliance with ASTM E-739-91

"Standard Practice for Statistical Analysis of Linearized Stress-Life (S-N) Fatigue Data."[16] The stress level of each test will be determined by calculating the maximum-bending stress according to the formula used for a four-point-bend specimen given in ASTM E-855–90 "Standard Test Method for Bend Testing of Metallic Flat Materials for Spring Applications."[17]

$$\sigma = 3\,Pa/bh^2 \tag{2}$$

where:

σ	=	Stress (MPa)
P	=	Applied load (N)
a	=	The distance between the inner and outer pins when the specimen is undeformed (mm) (see Figure 3)
b	=	Specimen width (m)
h	=	Specimen thickness (m)

The data was then plotted on a graph with the maximum stress and the number of cycles to failure along the vertical and horizontal axes, respectively, on a semilog scale in accordance with ASTM E-468-90 "Standard Practice for Presentation of Constant Amplitude Fatigue Test Results for Metallic Materials."[18] The linear curve fit and 90% confidence intervals were also plotted in accordance with ASTM E-739-91 "Standard Practice for Statistical Analysis of Linearized Stress-Life (S-N) Fatigue Data."[13] In the calculation using the linear curve model, the relationship between the stress and the sample life is given by the log-normal relationship:

$$Y = \hat{A} + \hat{B}X \tag{3}$$

where:

X	=	Log of sample lifetime (cycles)
Y	=	Stress (MPa)
$\hat{A}$	=	Estimator for curve fit Y (stress) intercept

$\hat{B}$ = Estimator for curve fit slope

$$\hat{B} = \frac{\sum_{i=1}^{k}(Xi - \overline{X})(Yi - \overline{Y})}{\sum_{i=1}^{k}(Xi - \overline{X})^2} \quad (4)$$

$\overline{Y}$ = Average of all Y values

Xi = Individual X value

Yi = Individual Y value

The equation for determining the confidence interval of the data is given by:

$$Y = \hat{A} + \hat{B}X \pm \sqrt{2F_p}\hat{\sigma}\left[\frac{1}{k} + \frac{(X - Xi)}{\sum_{i=1}^{k}(X - \overline{X})^2}\right]^{1/2} \quad (5)$$

where:

F_p = Statistical coefficient

$\hat{\sigma}$ = Square root of the population variance

$$\hat{\sigma}^2 = \frac{\sum_{i=1}^{k}(Yi - \hat{Y})^2}{(k-2)} \quad (6)$$

k = Number of data points

3.3.4 MICROSCOPY

All of the metallography and fracture surfaces that were examined by SEM were first cleaned for 5 minutes in an ultrasonic acetone bath, then rinsed with methanol, and dried briefly with a heat gun. Subsequently, the samples were placed in a Cambridge Instruments Model 360 Scanning Electron Microscope. Most of the images were taken at a working distance of 9 mm, and the accelerating voltage was maintained at either 15 keV or 20 keV. Energy dispersive X-Ray spectroscopy (EDS) was performed using an Oxford Instruments Model 7060 X-Ray detector and a Link ISIS acquisition and

processing software package for analyses in order to identify qualitatively the chemical composition of microstructural features on the samples.

4.0 Results and Discussion

4.1 Microscopy

4.1.1 As-Received Microstructure

As can be seen in Figure 5, the microstructure of the as-received 4340 steel is tempered martensite. Because of this fine microstructure, exact details could not be readily identified until the sample was examined with the aid of the SEM. In Figure 6, the higher magnification of the SEM allowed the small, needle-like structures to be readily identified, which indicated that the microstructure of the as-received specimens was composed of tempered martensite.

4.1.2 Laser-Coated Microstructure

A metallography sample was obtained from the untested portion of a laser-coated sample to identify the changes that the laser coating process creates in the base metal. This sample represented the cross-section of a laser-coated specimen, as presented by plane I in Figure 2, and was prepared in the same manner as the as-received metallography sample.

The Lot 1 metallography sample, as shown in Figure 7. The microstructure in the HAZ is fine martensite, but below the HAZ boundary, the microsctructure is tempered martensite. There is no Cr present, and the number of inclusions if very small.

The Lot 2 microstructure of the metallography sample looked very similar to the Lot 1 metallography sample, as shown in Figure 8.

The metallography sample from Lot 4 was very different from the other Lots in that all of the coating layer had not been removed, as seen in Figure 9. In the fusion line between the coating and the substrate, there are many inclusions and pores. It is possible that these inclusions are the mechanism that caused the premature failure of the Lot 4 specimens.

A complete mechanistic explanation of the fatigue behavior can be suggested, but is difficult to verify due to the difficulty in consistently machining the samples to tolerances of 25 microns. It was difficult to know how much of the HAZ, if any, had been removed when the coating was removed. As a result, the variation of microstructure as a function of depth and processing parameters cannot be evaluated. However, in their study of the laser surface melting of AISI 4340 steel, Fastow, Bamberger, Nir, and Landkof reported a drop in microhardness across the HAZ laser surface melted AISI 4340, and attributed it to a change in the microstructure from fine to coarse martensite.[21] A similar result was obtained in this study, as will be seen later.

4.2 Tensile Results

The results of the two tension tests that were conducted are shown in Figure 10. The 0.2% offset yield strength for this lot was 1,516 MPa. The average ultimate tensile strength of the two specimens was 1,830 MPa. The elongation of the samples was just under 12%. The curves show a yield point behavior that is not typical of AISI 4340 Steel.

4.3 Microhardness

The hardness data for the as-received material and Lot 1 are plotted against the depth of the sample away from the laser-coated surface in Figures 11-14, respectively. The depth of 0.000 mm on the figures represents the laser-coated surface.

In Figure 11, which represents the hardness data for the as-received samples, the hardness stays around a constant value of 500 Knoop. This is in contrast to the samples from Lot 1. As seen in Figure 12, which represents the hardness data for both planes I and II of the lot 1 sample, the hardness starts out around 575 Knoop and then climbs up to around 700 Knoop at the end of the HAZ. Over the next 200 microns, which represents the HAZ, the hardness values remain constant until dropping to 400 Knoop at

400 microns. At the end of the heat-affected zone, the hardness values climb back up to the value of 500 Knoop in the substrate and stay around this value for the remainder of the sample. The results of microhardness testing for Lots 1, 2, and 4 were similar to the results reported by Shuie and Chen, who conducted laser transformation hardening of 4340 with a CO_2 laser.[22]

For the Lot 2 specimen, as shown in Figure 13, the hardness values were taken in five columns at varying locations across the top surface of the specimen, and proceeding deeper into the specimen at regular intervals. The Lot 2 hardness data was similar to that of Lot 1. The hardness at the surface of the specimen reached a value of nearly 570 Knoop and quickly increased to a maximum of about 600 at a depth of 150 microns. Starting at about 200 microns, the hardness dropped to a minimum of about 370 Knoop at a depth of 400 microns, and then slowly recovered to the as-received value of 500 Knoop at a depth of 850 microns. The hardness data for the first 400 microns of all of the laser-processed samples showed considerable scatter, particularly the Lot 2 specimen, which appears to have two distinct peaks and two distinct drops in microhardness. This is due to the fact that some of the columns of hardness indentions cross through the region of the surface where two consecutive laser passes overlapped. Once the columns of indentions reached the areas that were unaffected by the LSA process, the hardness values became much less scattered.

The hardness data for Lot 4 is shown in Figure 14. The microhardness begins at a level of about 600 Knoop and increases slowly to a maximum of about 700 at a depth of 600 microns. The hardness then drops rapidly over the next 200 microns to about 425 Knoop, then slowly increases back to the nominal hardness of 500 Knoop of the as-received specimen at about 1500 microns. The Lot 4 sample returns to the nominal substrate hardness 500 microns deeper then either Lot 1 or Lot 2. This is consistent with the fractography and metallography results, which suggest that the Cr coating has not

been fully removed from the Lot 4 specimens, and also explains why the fatigue behavior of the Lot 4 samples was so different, as discussed later.

4.4 FATIGUE BEHAVIOR

The fatigue results are plotted in Figures 15 and 16. The as-received samples had a fatigue life of approximately 10,500 cycles at a stress level of 1,600 MPa, and when plotted on a log-normal plot of the cycles to failure vs. maximum stress, the fatigue life decreased linearly to a value of about 65,000 cycles at a maximum stress of 1,200 MPa. Below 1,144 MPa, the as-received samples did not fail within 1,000,000 cycles, and this is the stress value of the endurance limit for the as-received material.

The samples from Lot 1 behaved very similarly to the as-received samples at stress levels higher than 1,400 MPa, but somewhat better than the as-received samples at stress levels lower than 1,300 MPa. The endurance limit of the lot 1 samples was found to be 1,162 MPa, which was higher than the as-received endurance limit of 1,144 MPa. The data scatter for the lot 1 samples was very high, and as a result the confidence interval was not included on the graph of the data.

The Lot 2 samples behaved much like the Lot 1 samples. Over half of the samples that were run at maximum stress levels above 1,350 MPa fell within or above the confidence interval of the as-received samples. The data scatter, however, was high enough that the confidence interval was not included. The endurance limit for the Lot 2 samples was much better than that of either the as-received lot or Lot 1. The endurance limit of the Lot 2 samples was found to be 1,295 MPa.

The Lot 4 samples displayed a much poorer fatigue performance than all of the other lots. At every stress level above 1,050 MPa, the Lot 4 samples failed prior to 10^4 cycles. Lot 4 exhibited no endurance limit, even down to 600 MPa, which is about one half of the endurance limit of the as-received lot and Lot 1. The poor performance of this

lot of samples is attributed to the fact that all of the laser coating had not been removed, as has been previously discussed.

It should be noted that several samples from Lots 1 and 2 were discarded as outliers. In each case, when the fracture surface was examined in the SEM, the crack initiation site occurred at an area where the coating layer had not been fully removed. These areas all showed large concentrations of Cr, and the areas underneath the Cr-rich crack initiation site all showed signs of intergranular fracture, as shown in Figures 17 and 18. These samples also exhibited cracks in the boundary between the Cr-rich coating and the HAZ. This phenomenon has also been seen by Oñoro and Ranninger.[6]

The limited improvement in the fatigue performance of some of the lots can be attributed to two factors, the increase in hardness at the surface, which tends to resist crack initiation, and the softening of the subsurface region, which reduces the hardness and increases the resistance to crack propagation, as discussed later. The decrease in the crack propagation rates of the HAZ of a laser welded medium carbon steel was shown by Tsay, Chung and Chen.[11]

4.5 FRACTOGRAPHY

The fracture surfaces of representative samples from the as-received samples, and Lots 1, were examined with SEM. Micrographs of several of these fracture surfaces are presented in Figures 19 through 23. Crack initiation for the as-received samples, shown in Figure 19, occurred at or near inclusions that were either at the surface, or just beneath the surface. The as-received samples exhibited transgranular crack propagation, with no striations. Figure 20 is a close-up of Figure 19, which shows the inclusion that served as the crack initiation site for that sample.

The Lot 1 samples exhibited neither fatigue striations nor intergranular fracture, as shown in Figure 21. The crack initiation site is seen near an inclusion, which is at the surface, and the crack propagation mode is transgranular.

The fracture surface of the Lot 2 specimen was similar to the Lot 1 specimen. The crack initiated at an inclusion very near to the surface, as shown in Figure 22. The mode of crack propagation is transgranular, and there are no striations or intergranular fracture present.

The Lot 4 specimens showed markedly different behavior, as seen in Figure 23. The crack initiation site occured in a region where the Cr-CrB_2 has not been fully removed. When subjected to Energy Dispersive X-Ray Spectroscopy (EDS), this region was found to be Cr rich. There are also numerous particles and inclusions present in the Fe-Cr matrix. Directly below the Cr rich region is an area where the predominant mode of crack propagation is intergranular fracture.

5.0 CONCLUSIONS

As seen in the fatigue results, the HAZ itself does not have an adverse affect on the high-cycle fatigue performance of LSA processed AISI 4340 steel. In fact, some processing conditions actually improved the high-cycle fatigue performance of this alloy, although how much it improved the performance is difficult to quantify due to the difficulties that were encountered in trying to machine off all of the Cr-CrB_2 coating without disturbing the underlying substrate. This improvement can be attributed to two factors, the increase in hardness at the surface, which tends to resist crack initiation, and the softening of the subsurface region, which reduces the hardness and increases the resistance to crack propagation.

The fusion line between the coating layer and the substrate contains many inclusions, and is likely the cause of poor fatigue performance.

6.0 Potential Impact of Research

The results of the research could have an impact in widely ranging industries from the aerospace industry, to power generation, and the automotive industries. The LSA technology could allow designers to replace currently used, expensive corrosion and wear resistant alloys with less expensive, conventional alloys that have been modified by the LSA process to apply coatings that make them suitable in harsh environments.[27] Establishing the parameters that maximize the fatigue resistance of the HAZ of the PLD-treated AISI 4340, and understanding how the treatment affects the microstructure of the substrate will permit AISI 4340 to be used in corrosive and wear-intensive environments for which it is not currently suited.

7.0 FUTURE WORK

In order to have a complete understanding of the effects that are occurring, a larger and more comprehensive study could be undertaken at the conclusion of this research. Additional fatigue testing protocols could examine high-cycle tension fatigue, low-cycle fatigue, and fatigue crack growth behavior, and this testing could be conducted at elevated temperatures and in different environments. This would expand the base of fatigue crack growth work on unprocessed AISI 4340 that was performed by Liaw, Reax, and Donald.[28] Residual stress analyses could be performed to examine how the LSA process affects the residual stresses that are introduced during the resolidification of the melt zone and in the HAZ. These additional avenues of inquiry could produce a more complete picture of how LSA affects the behavior and performance of low-alloy, medium-carbon, high-strength steels.

REFERENCES CITED

1. A. Agarwal and N. B. Dahotre. "Synthesis of Boride Coating on Steel Using High Energy Density Process: Comparative Study of Evolution of Microstructure," *Materials Characterization*, vol. 42 (1999), 31-44.
2. K. L. Dahm, L. R. Jordan, J. Haase, and P. A. Dearneley. "Magnetron Sputter Deposition of Chromium Diboride Coatings," *Surface and Coatings Technology*, vols. 108-109 (1998), 413-418.
3. M. H. McCay, N. B. Dahotre, and J. A. Hopkins. "The Effect of Chromium and CrB_2 Additions on the Formation of Borides During Laser Surface Modification of Steel," *Surface Engineering in Materials Science I*, Eds. S. Seal, N. B. Dahotre, J. J. Moore, and B. Mishra, The Metallurgical Society of AIME, Warrendale, PA.
4. S. P. Gadag, M. N. Srinivasan, and B. L. Mordike. "Effect of Laser Processing Parameters on the Structure of Ductile Iron," *Metallurgical Transactions A,* vol. A196 (1995), 145-151.
5. N. B. Dahotre and K. Mukherjee. "Development of Microstructure in Laser Surface Alloying of Steel with Chromium," *Journal of Material Scien*ce, vol. 25, no. 1B: 445-454, Jan. 1990.
6. J. Oñoro and C. Ranninger. "Fatigue Behavior of Laser Welds of High-Strength Low-Alloy Steels," *Journal of Materials Processing Technology*, vol. 68 (1997), 68-70.
7. H. K. Lee, K. S. Kim, and C. M. Kim. "Fracture Resistance of a Steel Weld Joint Under Fatigue Loading," *Engineering Fracture Mechanics*, vol. 66 (2000), 403-419.
8. B. C. Kim, S. Lee, D. Y Lee, and N. J. Kim. "In Situ Observations on Tempered Martensite Embrittlement in an AISI 4340 Steel," *Metallurgical Transaction A*, vol. 22A (1991), 1889-1892.

9. J. R. Hwang, K. P. Peng, and C. C. Wang. "Effect of Second Phase on the Fatigue Crack Growth in AISI 4340 Steel," *Journal of Materials Science Letters*, vol. 15 (1996), 192-196.

10. J. R. Hwang, J. L. Doong, and C. C. Chen. "Fatigue Crack Growth in Laser Weldments of a Cold Rolled Steel," *Materials Transactions, JIM*, vol. 37, no. 8 (1996), 1443-1446.

11. L. W. Tsay, C. S. Chung, and C. Chen. "Fatigue Crack Growth of D6AC Laser Welds," *International Journal of Fatigue,* vol. 19, no. 1 (1997), 25-31.

12. U.S. Patent Number 5,985,056, Method for Laser Induced Improvement of Surfaces.

13. Annual Book of ASTM Standards, Standard Test Methods for Tension Testing of Metallic Materials, Information Handling Services, E 8-00b (2000).

14. Annual Book of ASTM Standards, Standard Test Method for Microhardness of Electroplated Coatings, Information Handling Services, B578-87 (2000).

15. Annual Book of ASTM Standards, Standard Test Method for Microindentation Hardness of Materials, Information Handling Services, E384-99 (2000).

16. Annual Book of ASTM Standards, Standard Practice for Statistical Analysis of Linearized Stress-Life (S-N) and Strain-Life (ε-N) Fatigue Data, vol. 03.01, E739-91 (2000), 599-605.

17. Annual Book of ASTM Standards, Standard Test Methods for Bend Testing of Metallic Flat Materials for Spring Applications Involving Static Loading, vol. 03.01, E855-90 (2000), 640-647.

18. Annual Book of ASTM Standards, Standard Practice for Presentation of Constant Amplitude Fatigue Test Results for Metallic Materials, vol. 03.01, E468-90 (2000), 481-486.

19. G. F. VanderVoort. *Metallography: Principles and Practice,* 1984, Material Park: ASM International, 1999.

20. Y. C. Ku. *Deflection of Beams for all Spans and Cross Sections,* 1986, McGraw-Hill, Inc., NY.

21. M. Fastow, M. Bamberger, N. Nir, and M. Landkof. "Laser Surface Melting of AISI 4340 Steel," *Materials Science and Technology*, vol. 6 (1990), 900-904.

22. K. Shiue and C. Chen. "Laser Transformation Hardening of Tempered 4340 Steel," *Metallurgical Transactions A*, vol. 23A (1992), 163-170.

23. C. L. Briant. "Role of Carbides in Tempered Martensite Embrittlement," *Materials Science and Technology*, vol. 5 (1989), 138-147.

24. J. R. Hwang and C. P. Fung. "Effect of Electron Beam Surface Hardening on Fatigue Crack Growth in an AISI 4340 Steel," *Surface and Coatings Technology*, vol. 80 (1996), 271-278.

25. K. Sridhar and A. S. Khanna. "Laser Surface Heat Treatment," *Lasers in Surface Engineering,* N. B. Dahotre, Ed., ASM International, Materials Park, OH. 1998.

26. E. Lugshceider and I. Kvernes. "Thermal Barrier Coatings: Powder Spray Process and Coating Technology," *Intermetallic and Ceramic Coatings,* N. B. Dahotre, Ed. Marcel Dekker, Inc., NY, 1999.

27. M. Riabkina-Fishman and J. Zahavi. "Laser Alloying and Cladding for Improving Surface Properties," *Applied Surface Science*, vol. 106 (1996), 263-267.

28. P. K. Liaw, T. R. Leax, and J. K. Donald. "Fatigue Crack Growth Behavior of 4340 Steels," *Acta Metallurgica,* vol. 35 (1987), 1415-1432.

APPENDIX

Table 1. Composition Range of AISI 4340 Steel in Weight Percent

C	Mn	P	S	Si	Ni	Cr	Mo	Fe
0.38-0.43	0.6-0.8	0.035	0.04	0.15-0.35	1.65-2.00	0.7-0.9	0.2-0.3	Bal.

Table 2. Nominal Properties of As-Received (Quenched and Tempered) AISI 340 Steel

Tensile Strength MPa (ksi)	Yield Strength MPa (ksi)	Elongation (%)	Reduction of Area (%)	Rockwell "C" Hardness	Brinell Hardness	Knoop Hardness (HK 100 gf)*
1,830 (266)	1,516 (220)	11.5	46	48.5	469	500

* gf = grams force

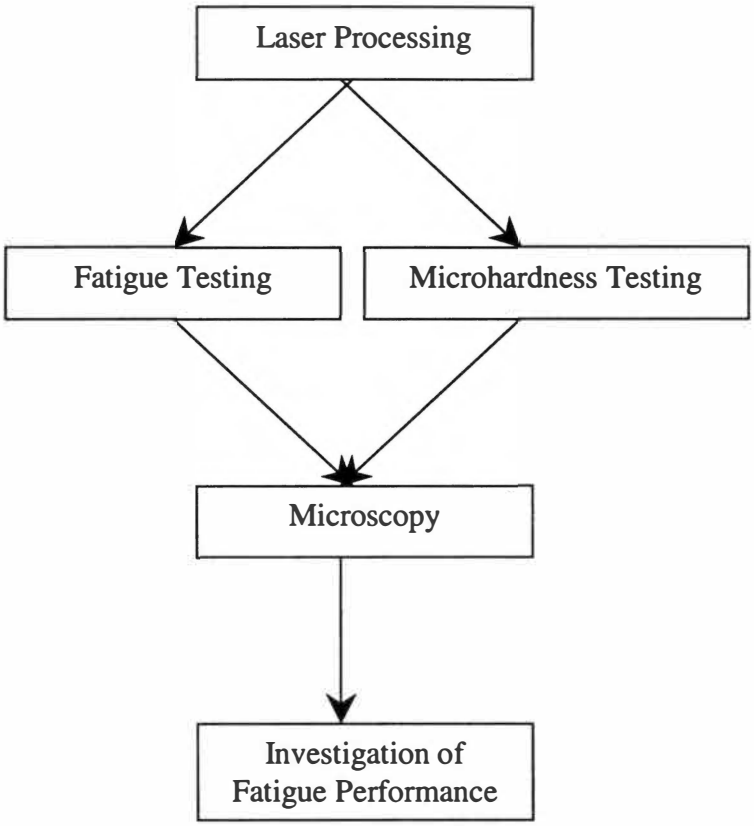


Figure 1. Schematic of Research

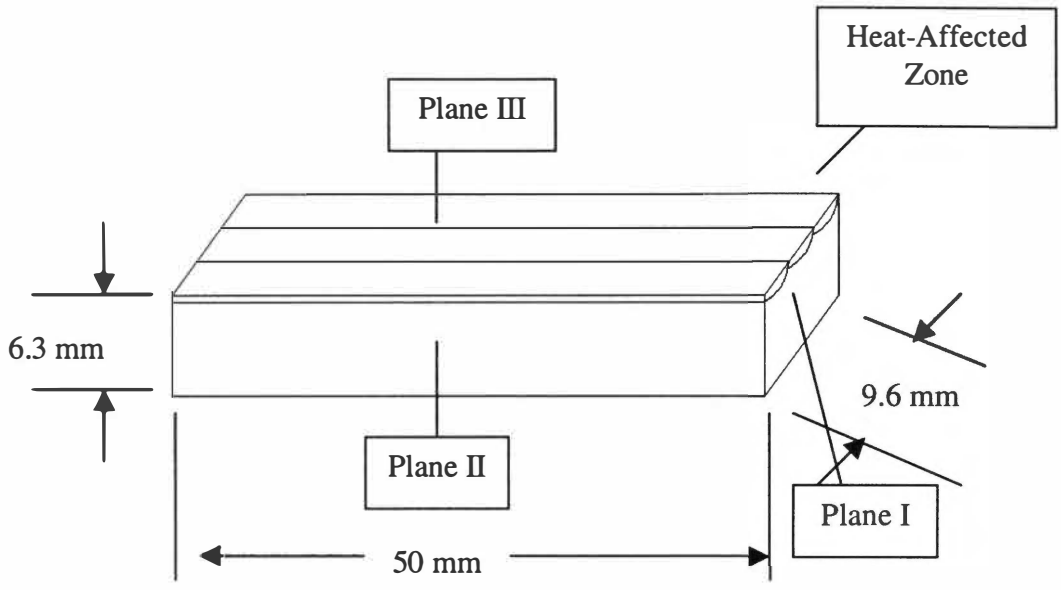


Figure 2. Sketch of Specimen Geometry Detailing Dimensions and Geometric Planes of Interest

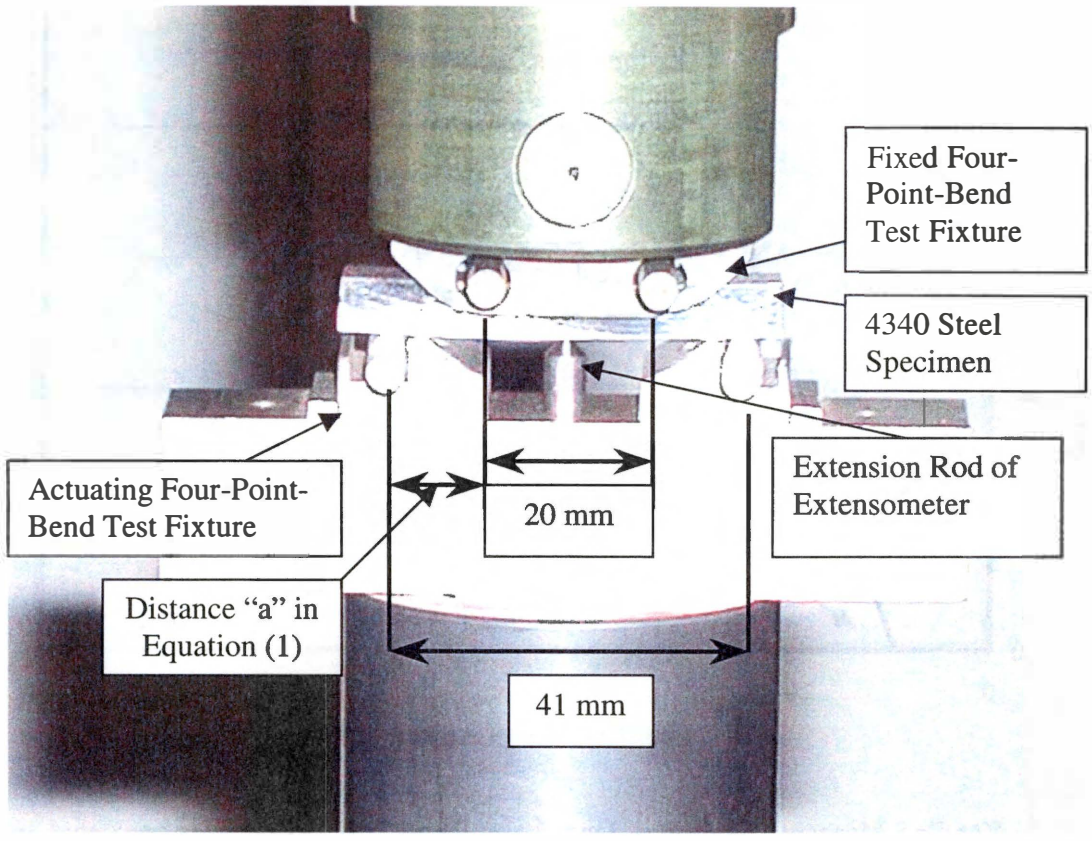


Figure 3. Test Fixture Setup with Specimen Installed

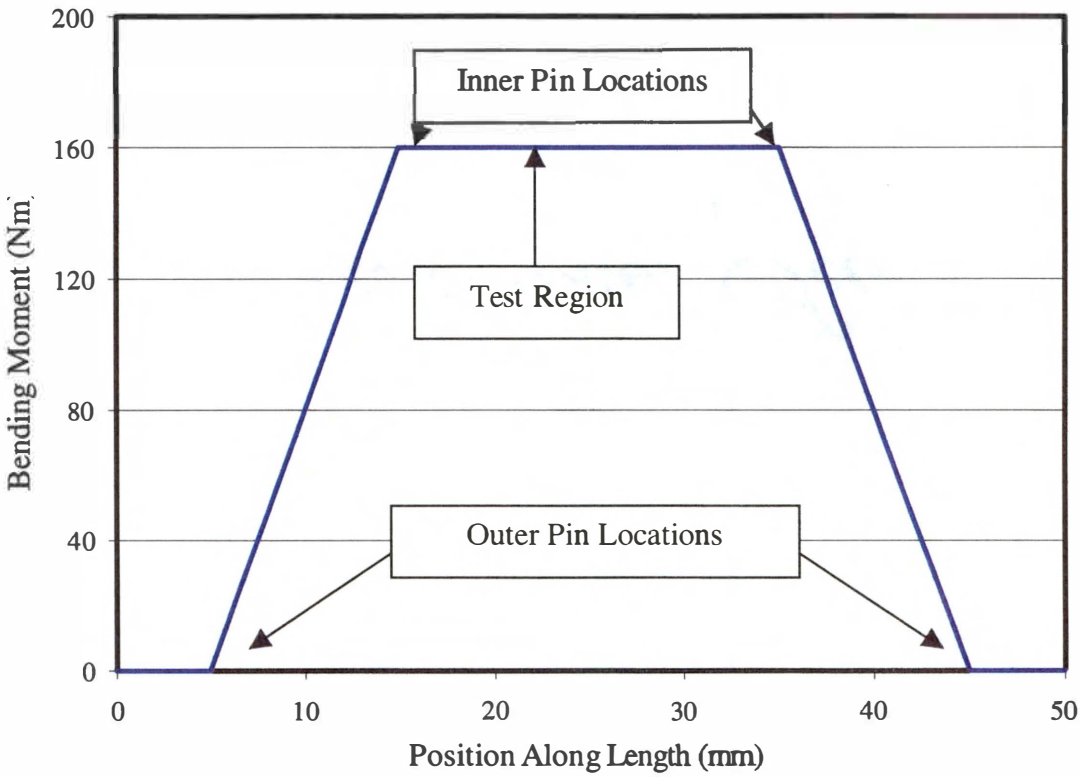


Figure 4. Bending Moment Diagram of Four-Point-Bend Test. The values presented are for a typical specimen.

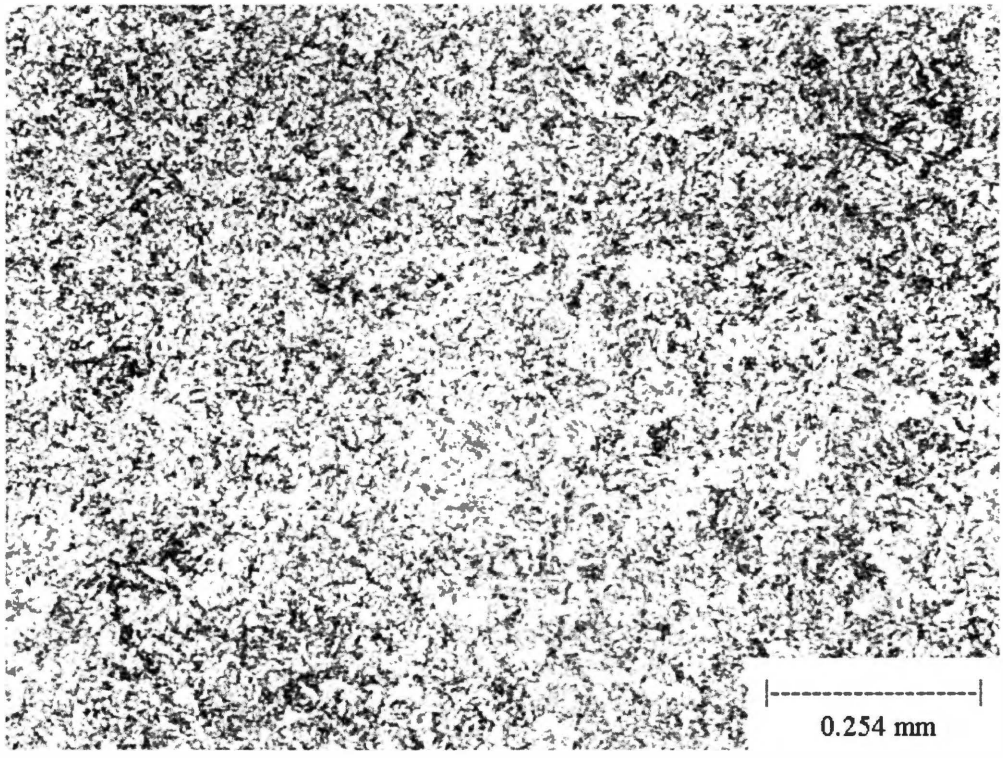


Figure 5. Optical Micrograph of an As-received, Untested Specimen Etched with 2% Nital. This cross-section, represented by plane I, shows a tempered martensite microstructure.

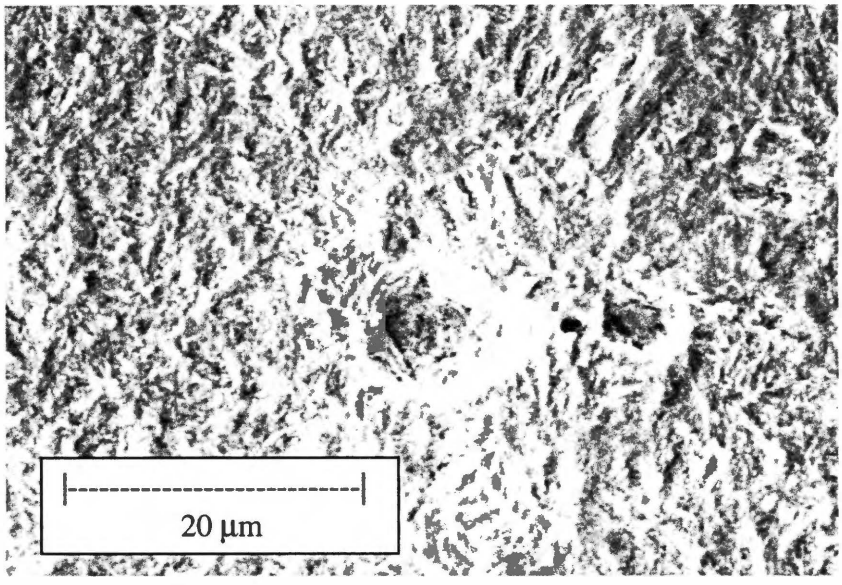


Figure 6. SEM Micrograph of an As-Received, Untested Specimen Etched with 2% Nital. This cross-section, represented by plane I, shows the tempered martensite microstructure.

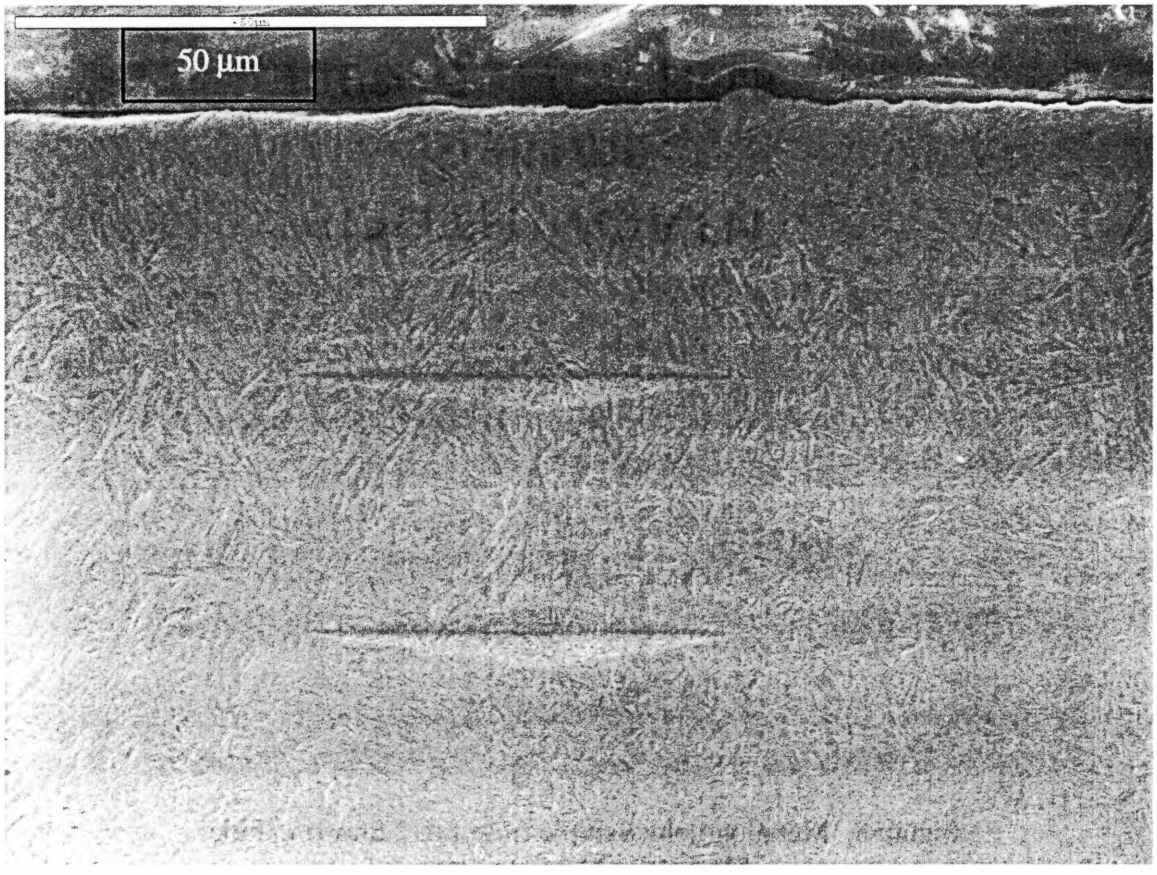


Figure 7. Metallography Specimen of LC18 from Lot 1. The specimen has been etched in 2% Nital. The microstructure is martensite.

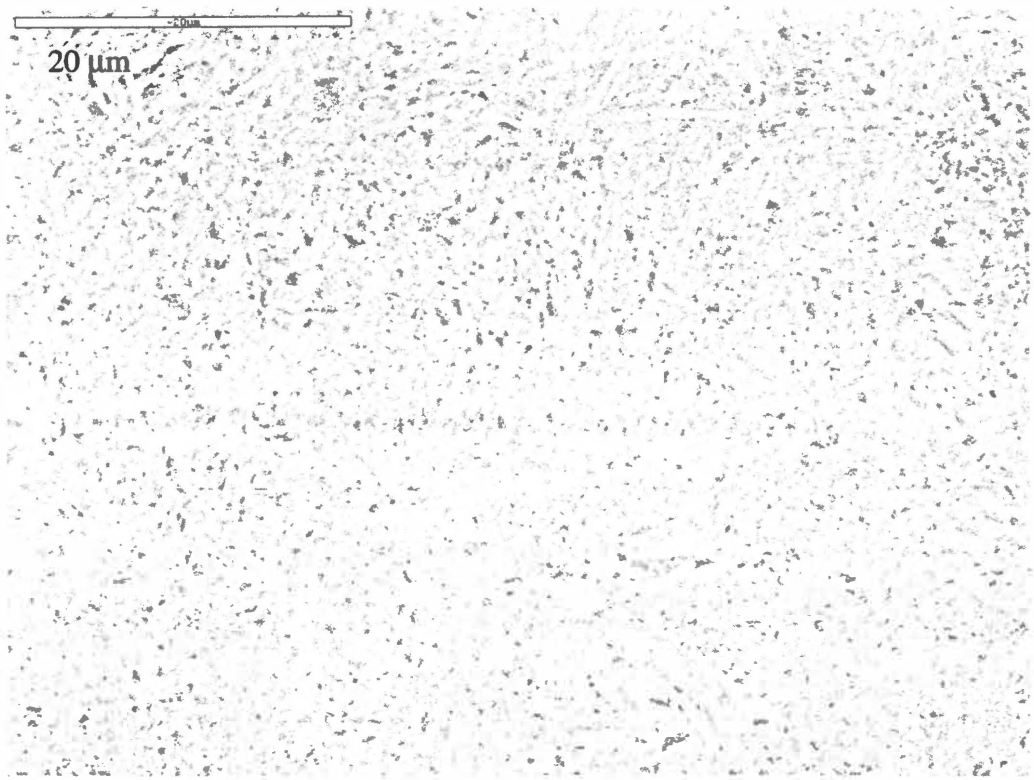


Figure 8. Metallography Sample from Lot 2 Showing Fine Martensite Microstructure

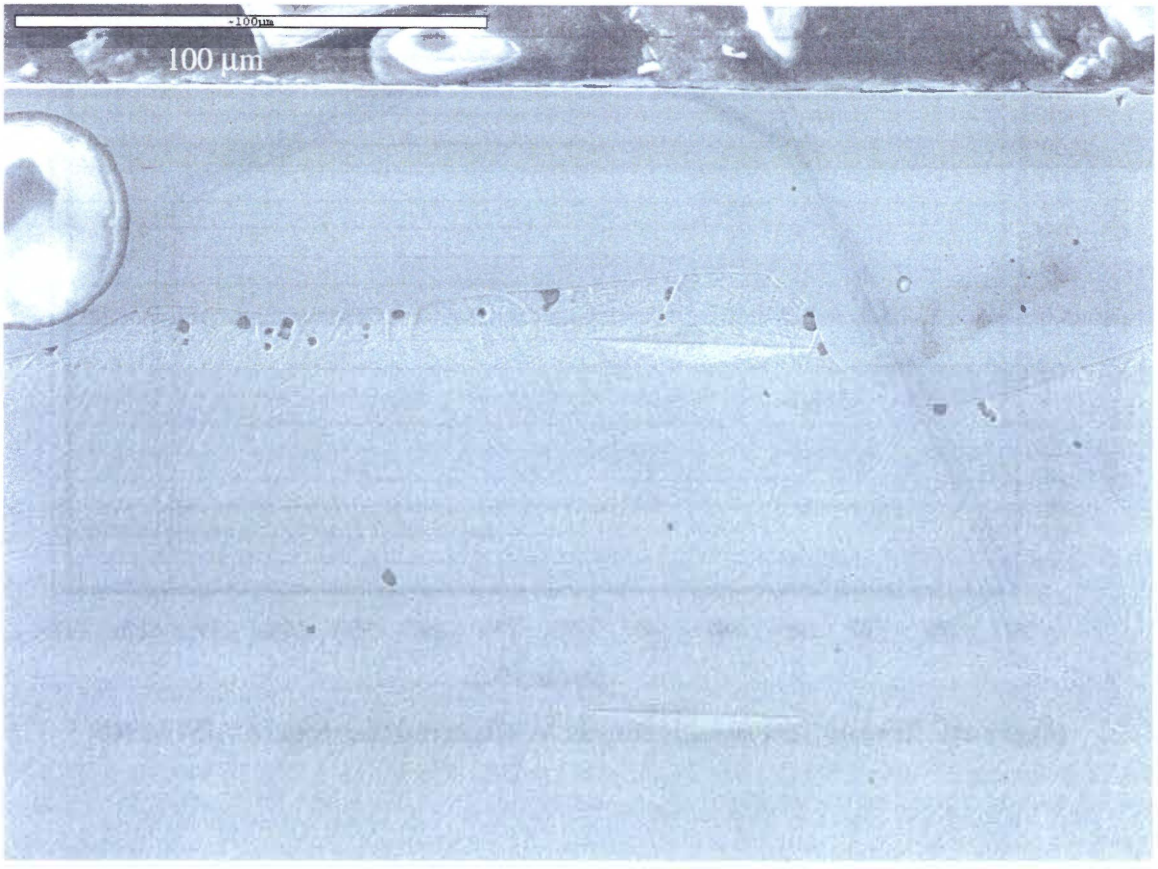


Figure 9. A Metallography Sample from Lot 4. Note the Cr-rich region at the top of the image, and the inclusions in the Cr-rich region and in the boundary with the substrate.

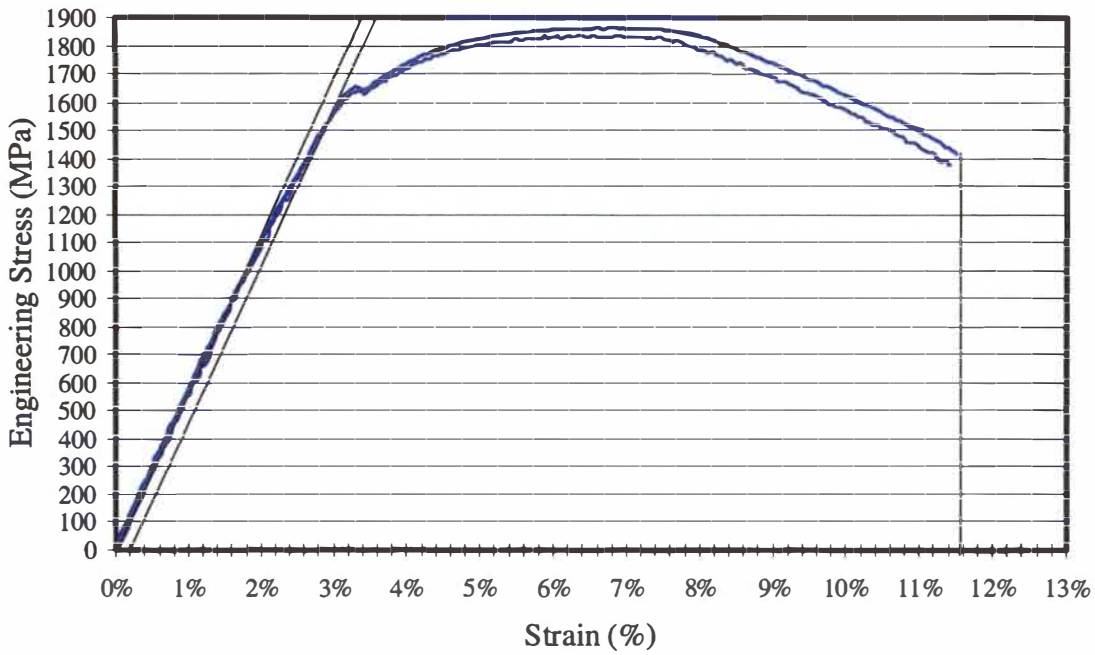


Figure 10. Tensile Test Results for the As-Received Samples of AISI 4340

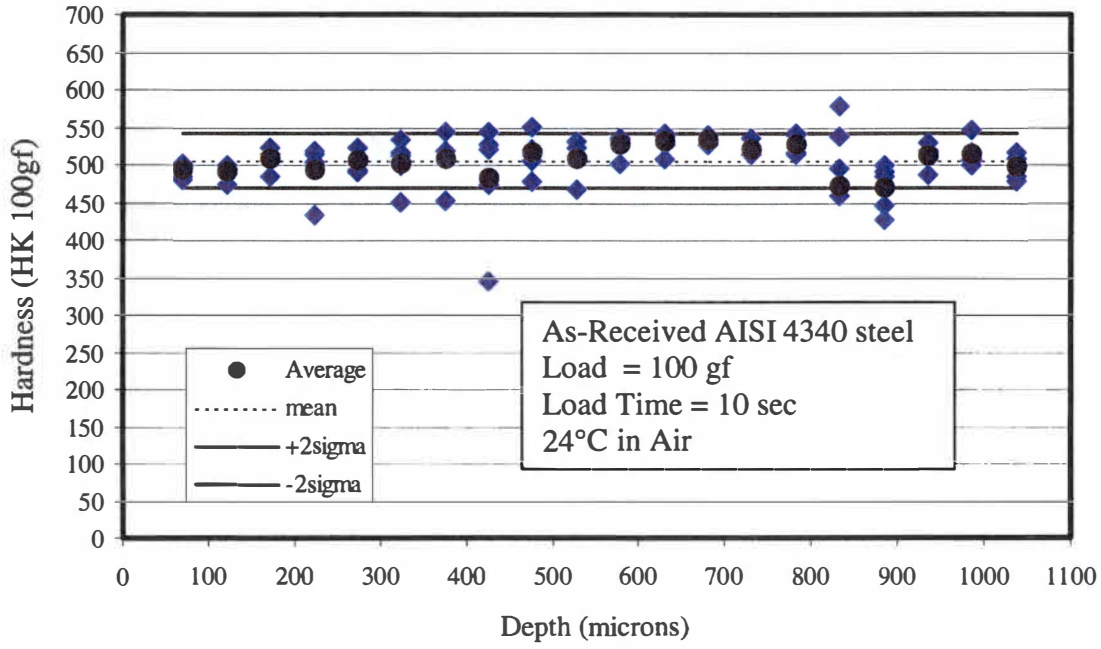


Figure 11. Knoop Hardness Values for an As-received Sample. Hardness values for planes I and II are given. A test load of 100 gf was applied for 10 seconds.

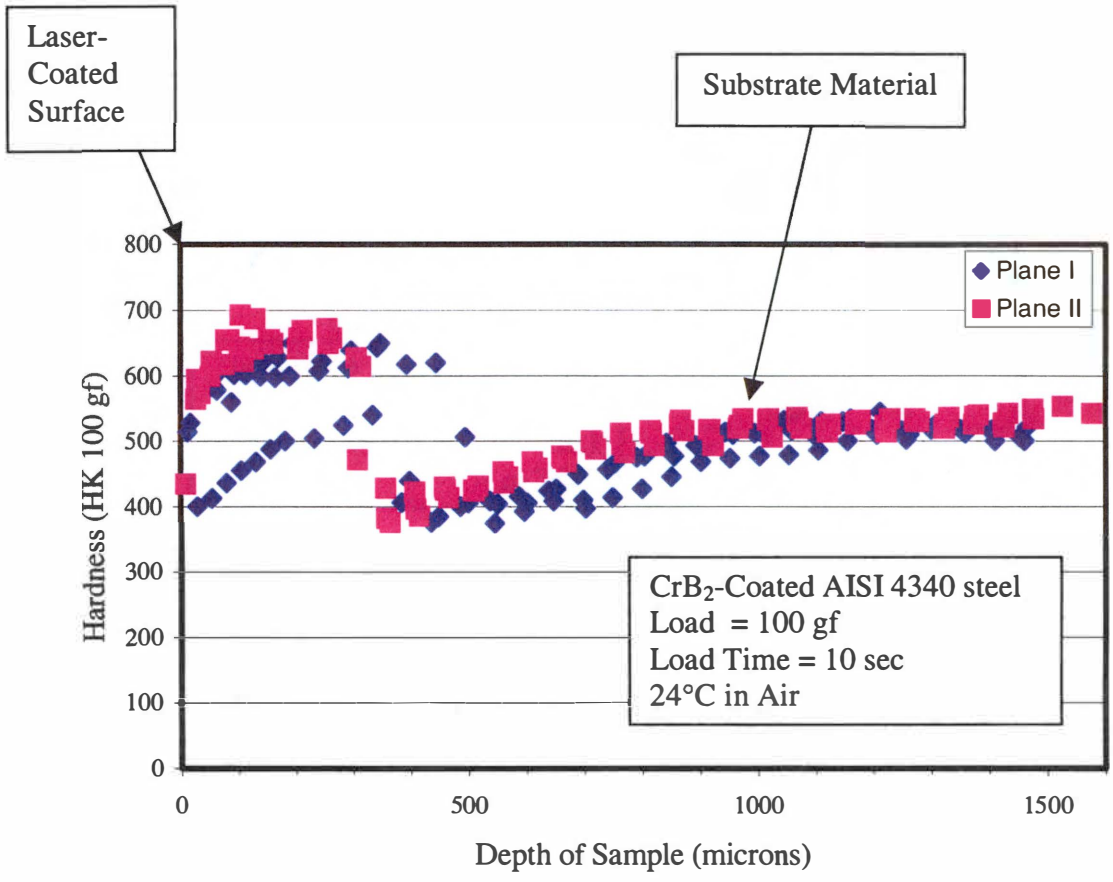


Figure 12. Knoop Hardness Values for a Lot 1 Sample. Hardness values for planes I and II are given. A test load of 100 gf was applied for 10 seconds.

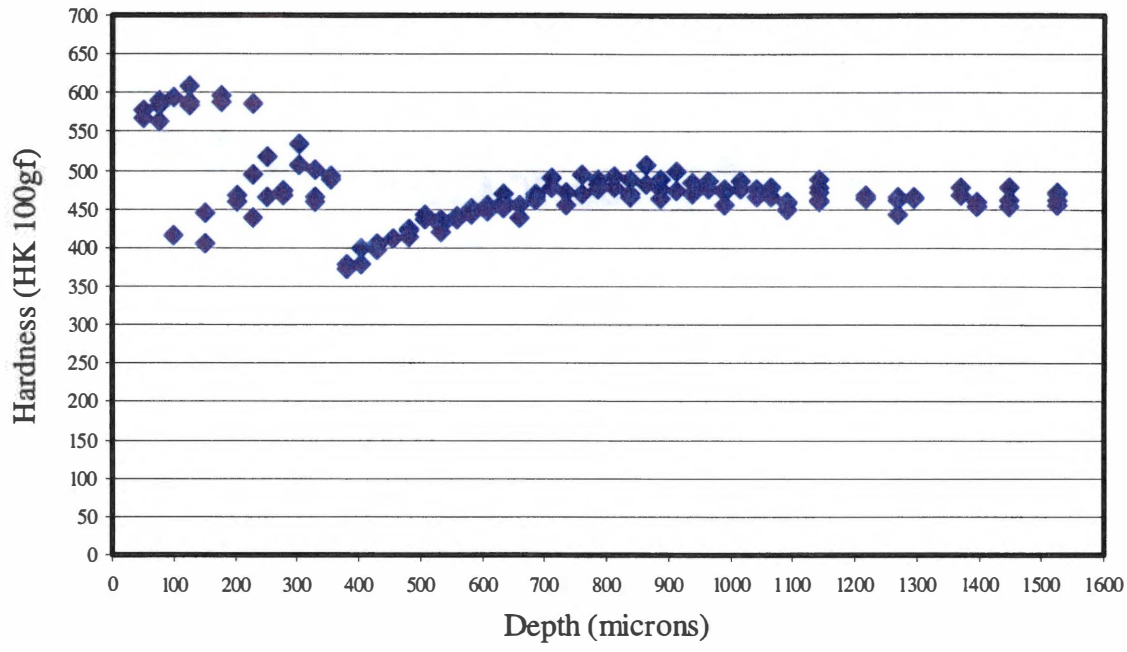


Figure 13. Knoop Hardness Values for a Lot 2 Sample. Hardness values for plane I are given. A test load of 100 gf was applied for 10 seconds.

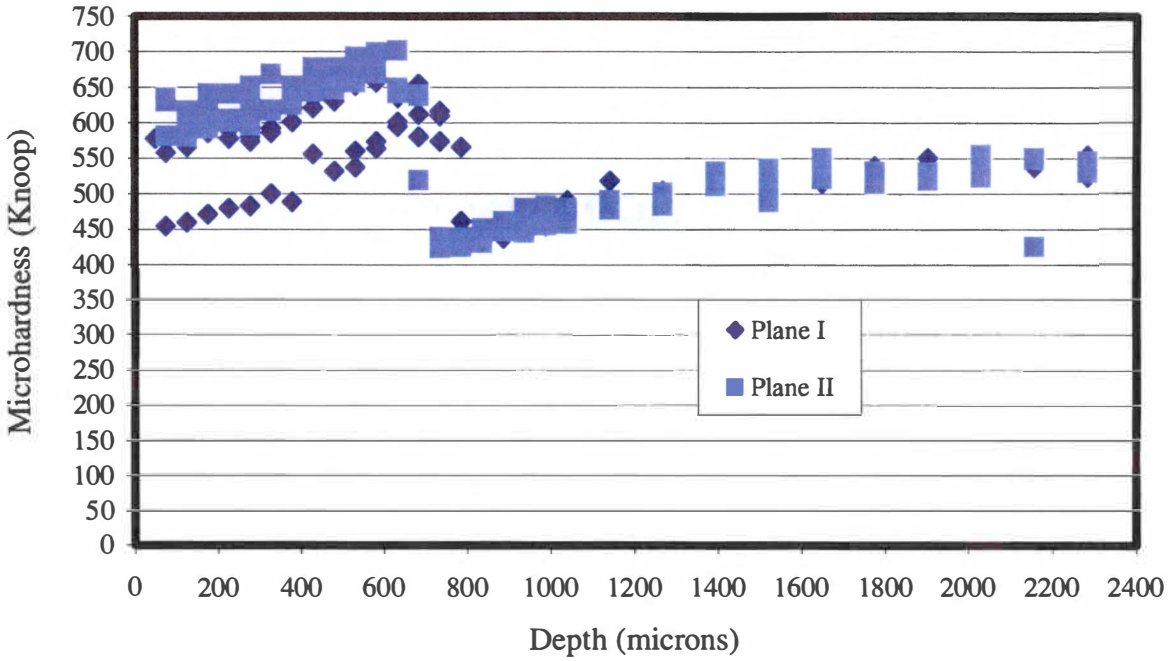


Figure 14. Microhardness Data for Lot 4. Hardness values for planes I and II are given. A test load of 100 gf was applied for 10 seconds.

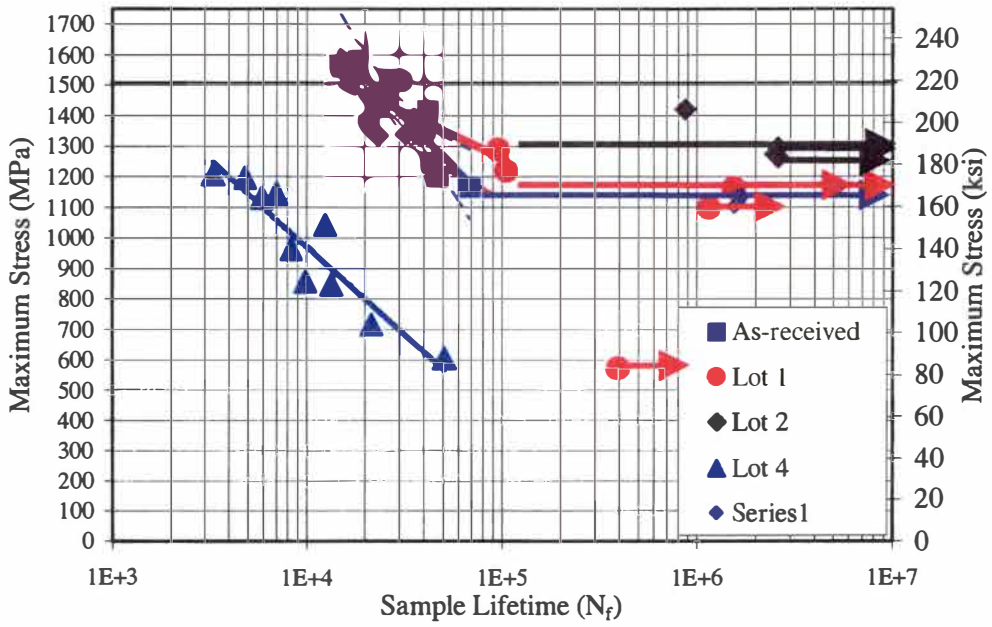


Figure 15. High-Cycle Fatigue Data for All Four Lots

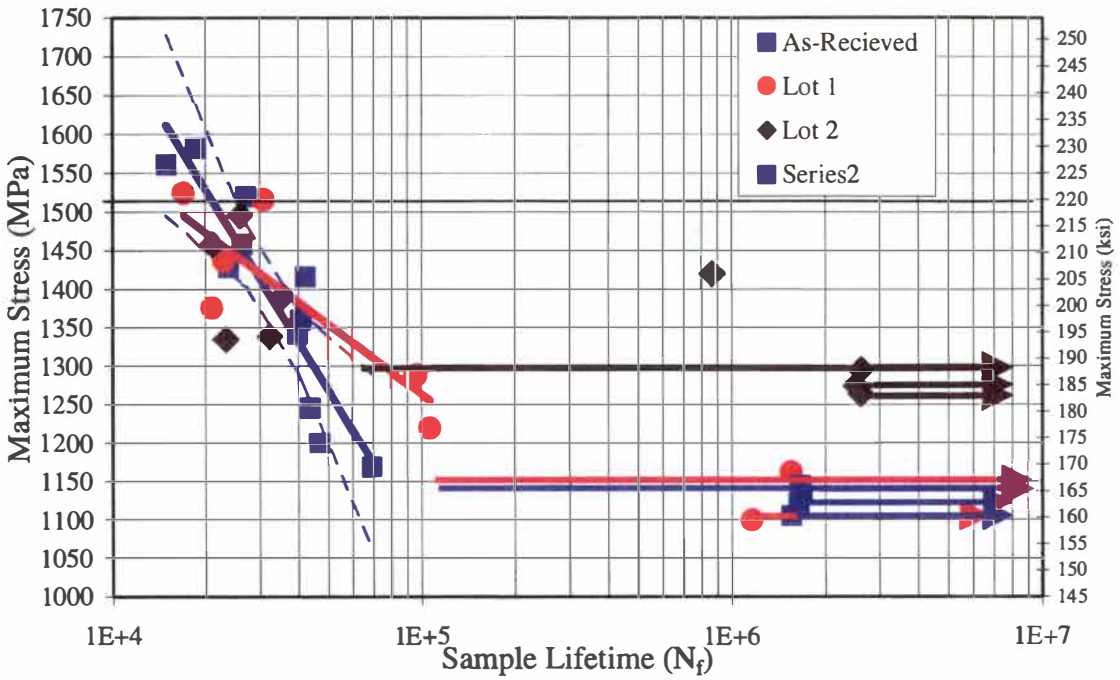


Figure 16. High-Cycle Fatigue Data Showing Only the As-Received Lot, Lot 1 and Lot 2

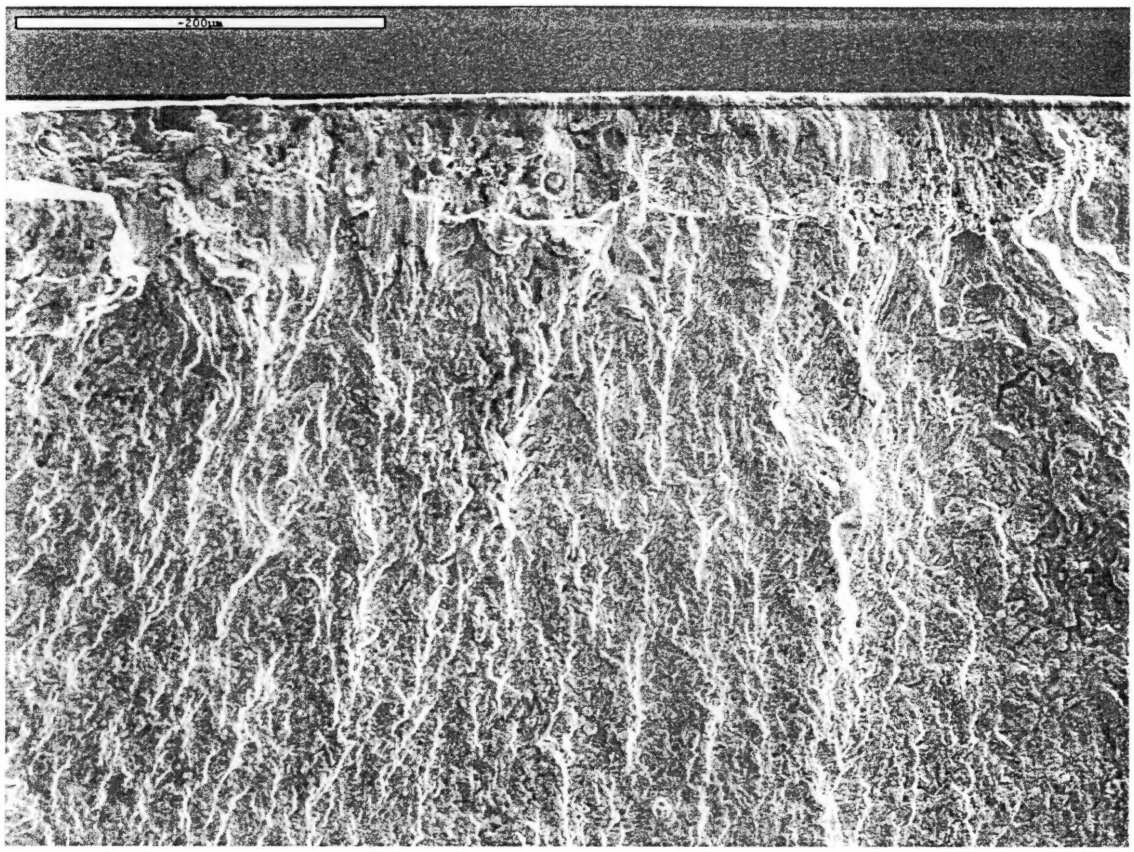


Figure 17. Fractograph of LC36. This specimen is an outlier from Lot 2. The scalloped region at the top of the image is Cr rich, as are the inclusions.

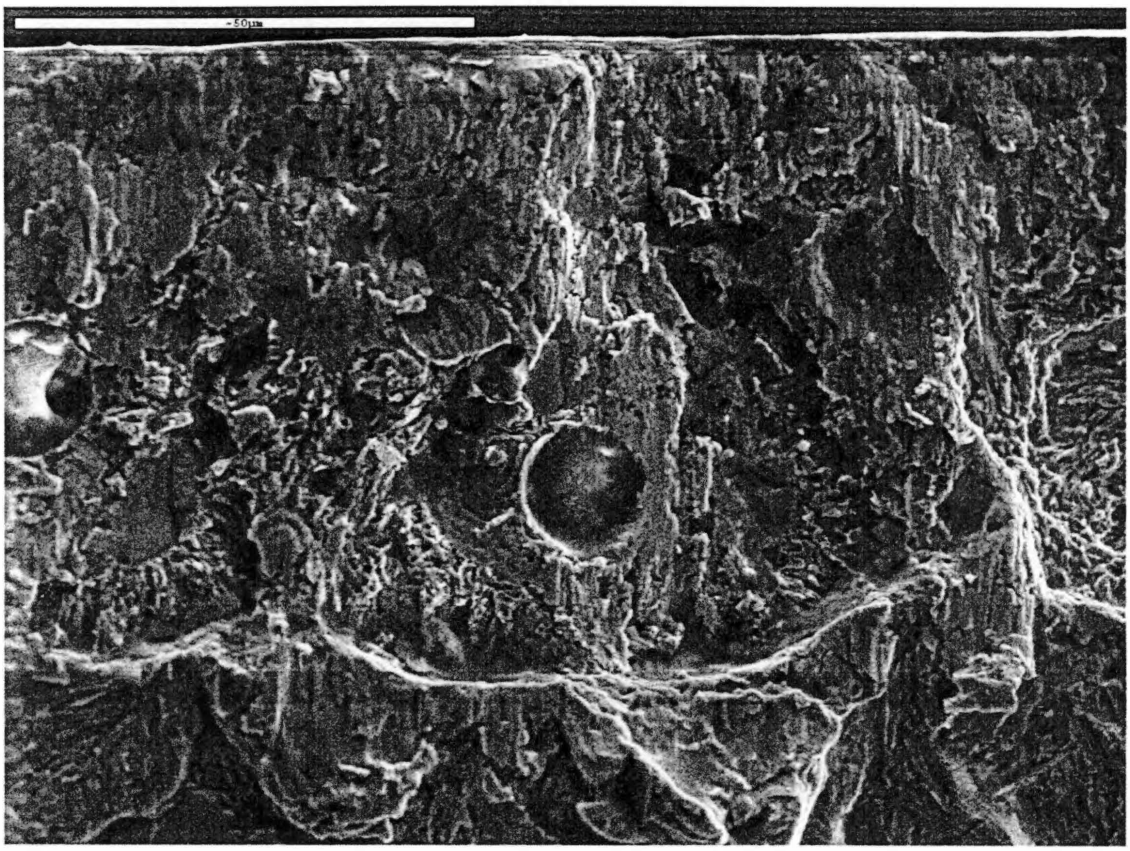


Figure 18. A Higher Magnification of Figure 17. Two large inclusions in the Cr-rich matrix are shown.

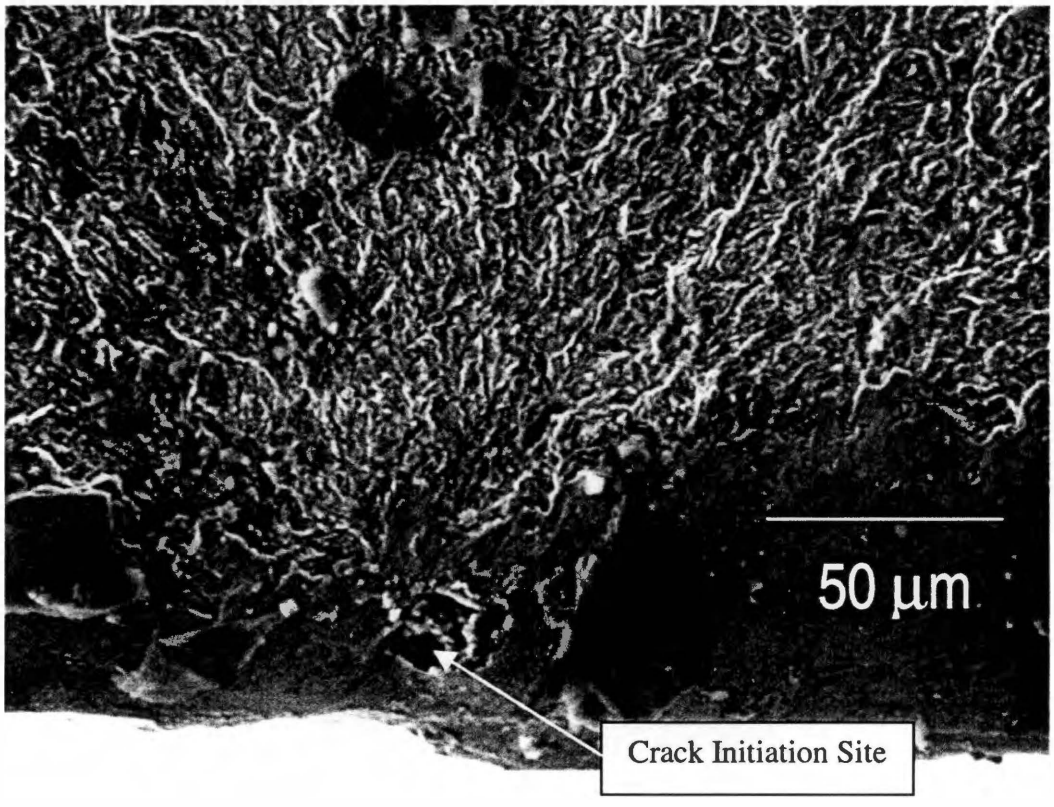


Figure 19. Fifty Micron SEM Micrograph of an As-Received Specimen. This cross-section, represented by plane I, shows the missing inclusion that acted as the crack initiation site for the specimen.

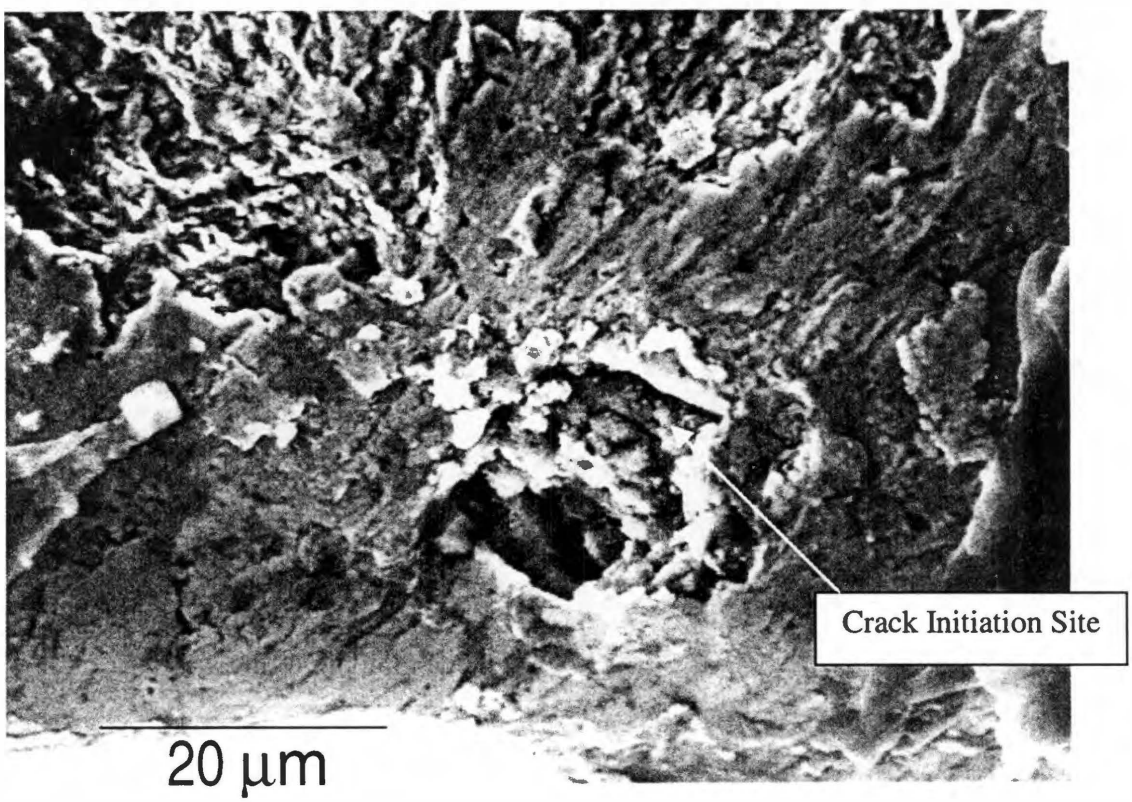


Figure 20. Twenty Micron SEM Micrograph of an As-Received Specimen. This cross-section, represented by plane I, shows an enlarged view of the missing inclusion that acted as the crack initiation site for the specimen in Figure 11.

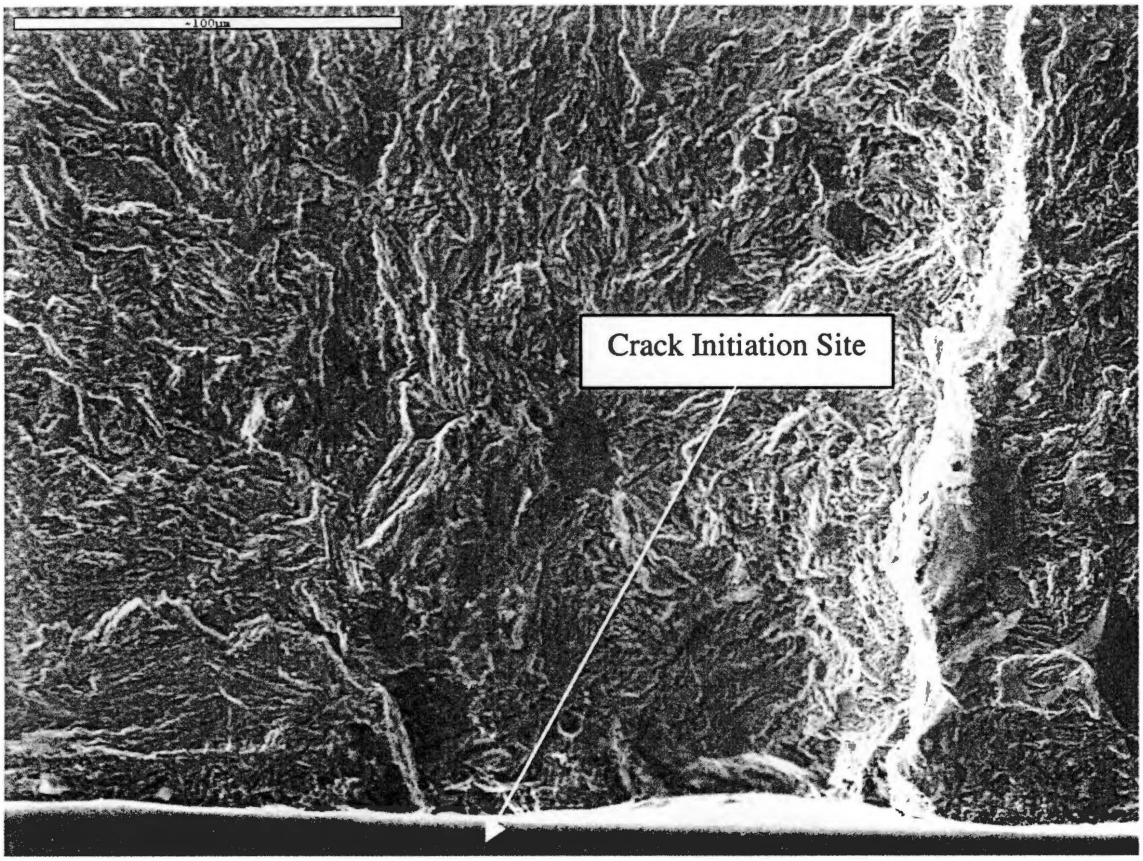


Figure 21. SEM Micrograph of a Laser-Coated Specimen from Lot 1. This cross-section of the crack initiation site, represented by plane I, shows the absence of striations and intergranular cracking, common to Lot 1 test specimens.

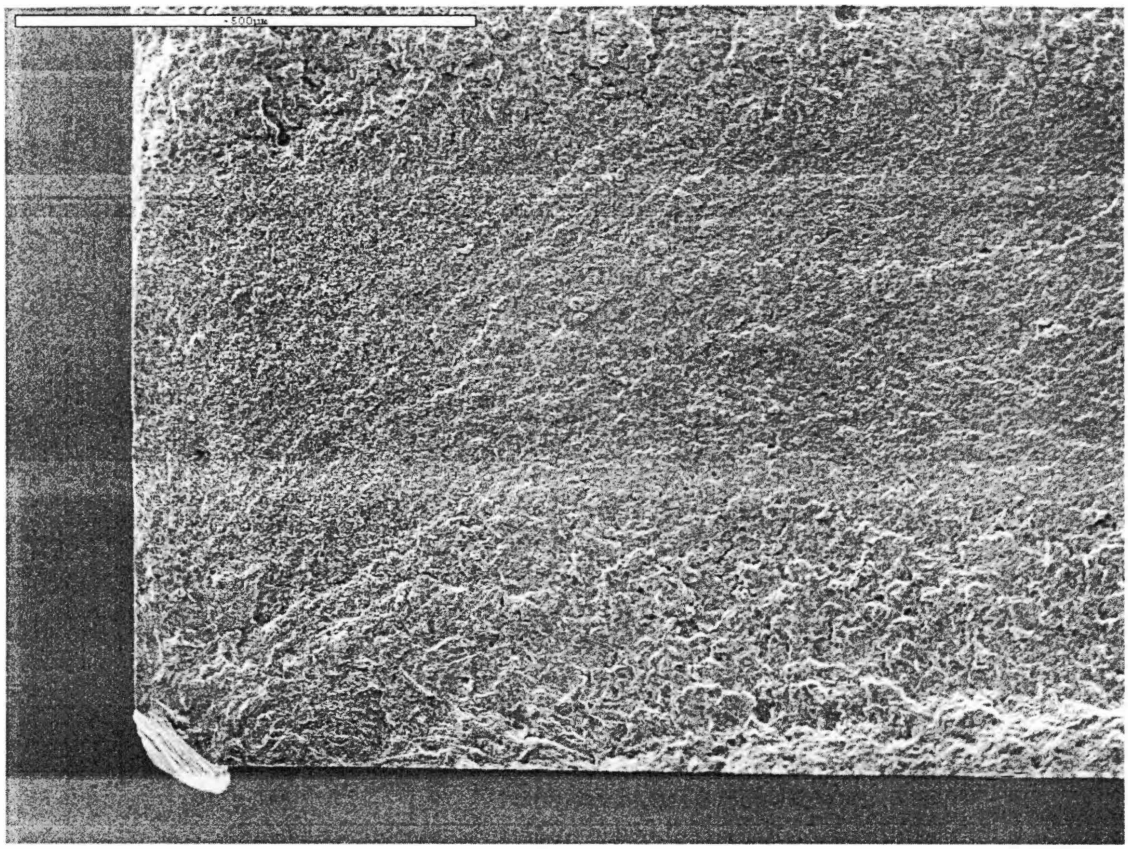


Figure 22. Fracture Surface of LC38, a Lot 2 Specimen. Crack initiation occurs in the bottom left corner near an inclusion just below the surface, and propagates transgranularly.

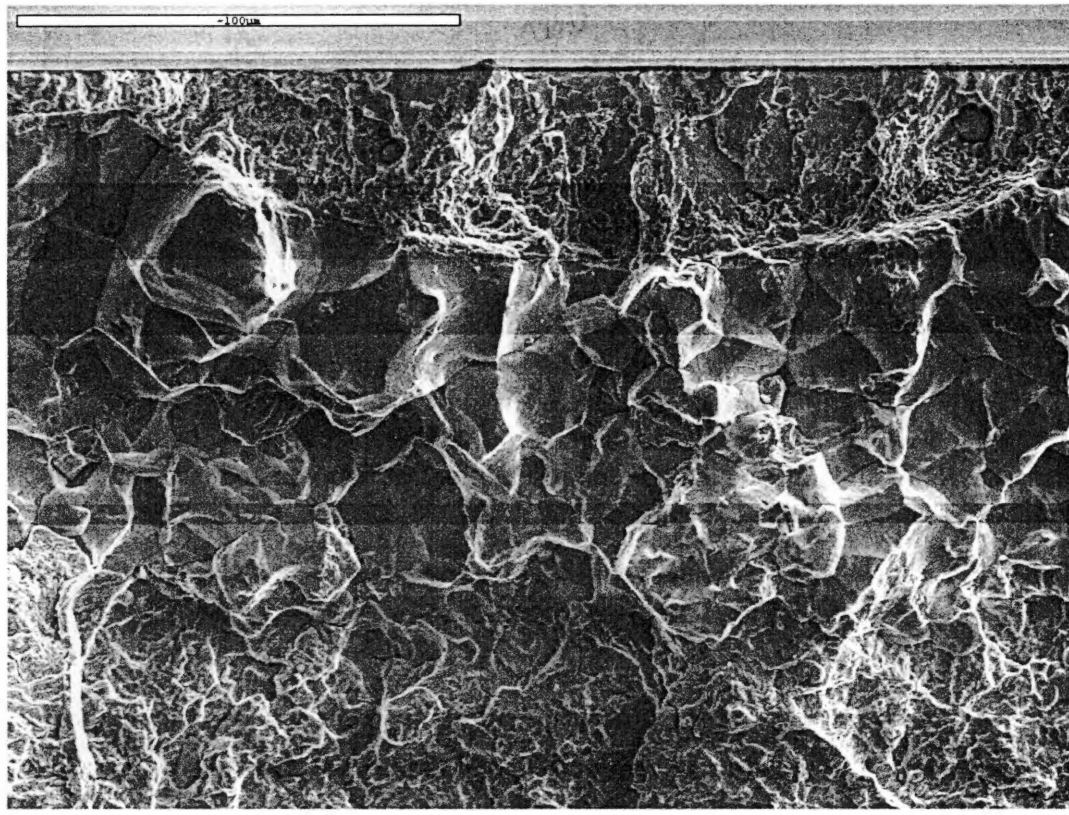


Figure 23. A Fractograph of LC38, a Lot 4 Specimen. Note the scalloped area at the top of the specimen. The Cr-rich region served as the crack initiation site, and there is a significant amount of intergranular crack propagation in the substrate.

VITA

Robert M^{c}Daniels graduated from Oakland High School in Murfreesboro, TN, in 1985. He attended the University of Tennessee from 1985 until 1990, when he joined the United States Marine Corps. He served on active duty in the Marine Corps from 1990 until 1994, when he transferred to the USMC Reserve, where he currently serves as a Staff Sergeant in Delta Co., 4th CEB.

He received his B.S. in Engineering Science from the University of Tennessee in May of 1996. He worked for MINCO/ Insul-Therm as a shift leader and Process Engineer from 1997 until 2000, when he returned to the University of Tennessee. In addition to his work on LSA, he has authored or co-authored several publications on the fatigue behavior of superalloys, and given presentations at regional and national conferences.

3785 2850 50
98-07-02 MRB